analytical chemistry

Article

pubs.acs.org/ac

A High-Sensitivity, Integrated Absorbance and Fluorescence Detection Scheme for Probing Picoliter-Volume Droplets in Segmented Flows

Tianjin Yang, Stavros Stavrakis,* and Andrew deMello*

Institute for Chemical and Bioengineering, Department of Chemistry and Applied Biosciences, ETH Zürich, Vladimir Prelog Weg 1, 8093 Zürich, Switzerland

Supporting Information

ABSTRACT: Droplet-based microfluidic systems that incorporate flowing streams of pL-volume droplets surrounded by a continuous and immiscible carrier phase have attracted significant recent attention due to their utility in complex chemical and biological experimentation. Analysis of pL droplets, generated at kHz frequencies and moving at high linear velocities, is almost exclusively achieved using fluorescence-based detection schemes. To extend the applicability of such optical detection schemes, we herein report the development of a simple and cost-effective optofluidic platform, integrating liquid-core PDMS waveguides, that allows the accurate measurement of absorbance within individual pL-volume droplets moving within segmented flows. Using such an approach, differential measurements of "sample "and "reference" droplets can be acquired at 1 kHz and yield detection limits of 400 nM for fluorescein in water. Significantly, the presented technique enables simultaneous fluorescence and absorbance interrogation of rapidly moving droplets in a fully automated manner. Proof of principle is demonstrated through the titration and monitoring of pH gradients in real time.

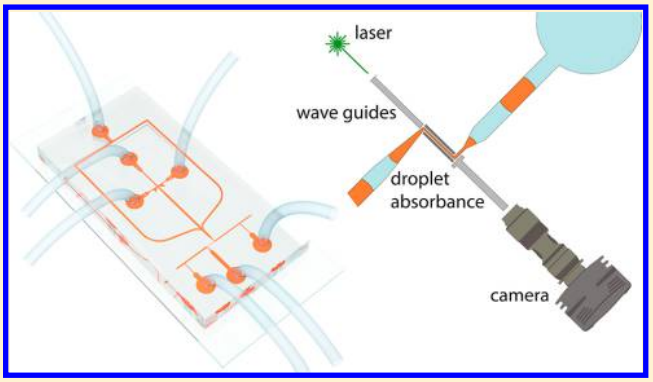

The advent of chip-based microfluidic systems has transformed the experimental landscape of chemical and biological science by allowing the accurate and precise control of fluids on small spatial and temporal scales. Such abilities have in turn engendered enormous improvements in analytical efficiency, throughput, cost per experiment, functionality, and system automation. Due to the fact that instantaneous volumes within microfluidic systems are typically within the fL−nL range, laser-induced fluorescence (LIF) methods represent the most commonly used detection schemes, due to their exquisite sensitivity and selectivity, noninvasive nature and low mass/concentration limits-of-detection.[1−6] While LIF-based techniques are routinely used to detect and probe molecular populations down to the single molecule level, they require that the analyte under study has either a high intrinsic fluorescence quantum efficiency or can be chemically modified with an appropriate extrinsic fluorophore. Conversely, UV−vis (absorption) spectroscopy is a ubiquitous and label-free detection technique for the quantitative analysis of almost all organic compounds exhibiting a degree of conjugation.[7−9] Unfortunately, the integration of absorbance detection within microfluidic systems is hindered by the simple fact that optical pathlengths are typically 2−3 orders of magnitude smaller than those encountered on the macroscale. Since absorbance is directly proportional to the optical path length, such reductions have precluded the widespread adoption of absorbance-based measurements in most small volume applications.

Unsurprisingly, much activity has focused on addressing such path length limitations, while ensuring that detector bandwidths are not significantly compromised (a critical requirement when performing separations in microfluidic formats). For example, the "single pass beam" approach has been implemented in a number of embodiments in continuous flow systems, by optically interrogating sample along the length of the microchannel and thus extending pathlengths to several mm.[10,11] Related strategies have also used modifications in channel geometries to create U- or Z-shaped detection cells, similarly increasing the optical path length at the point of analysis.[12−15] That said, even with extended optical pathlengths, reported detection limits are typically in the mid- to low-micromolar range.[15] More recently, an optofluidic single pass platform incorporating an optical modulator and state-of-the-art CCD detector was successful in detecting 13 μM solutions of methylene blue using an optical path length of only 28 μm, albeit at frame rates of only 4 Hz.[16] It should be noted that multireflection formats have also been shown to be successful in extending concentration detection limits down to the

Received: August 29, 2017
Accepted: November 9, 2017
Published: November 9, 2017

DOI: 10.1021/acs.analchem.7b03526
Anal. Chem. 2017, 89, 12880−12887

nanomolar range by reflecting excitation light several times through the sample volume to extend the interaction length.[17,18] To address sensitivity issues, a number of recent studies have adopted cavity-enhanced absorption spectroscopy (CEAS) as a route to extending optical pathlengths without increasing sample volumes. A representative example of such an approach was reported by Rushworth et al., who designed a cavity-enhanced absorbance detector leveraging a multi pass optical scheme and a broadband reflector film.[19] Significantly, adoption of such a configuration enhanced the absorption path length over 20 times and enabled micromolar range detection limits with an optical path length of only 50 μm.

Droplet-based microfluidic systems have proved to be of wide ranging utility in the performance of high-throughput chemical and biological experiments. By encapsulating and isolating reagents within micron-sized droplets, millions of assays or reactions can be processed in a parallel fashion and on ultrashort time scales. When compared to more established continuous-flow formats, droplet-based systems possess a number of critical advantages with respect to throughput, experimental robustness, ease of component integration, control of mass transport, and the ability to perform massively parallel experiments. That said, the detection of molecular species within the pL−nL volumes that characterize microfluidic droplets is particularly challenging due to the dearth of available sample and the fact that, under standard conditions, sizable numbers of droplets are moving at appreciable velocities (greater than 1 cm/s) through the system.[20] Moreover, the study of dynamic processes imposes additional constraints on the detection method, typically requiring multiple measurements of a given droplet over a period of time that may be as short as a few milliseconds. To this end, a small number of recent studies have focused on the development of absorbance-based detection schemes for probing segmented flows at the single droplet level. For example, Vallance and co-workers used cavity ring-down spectroscopy to quantify absorption within droplets, affording concentration detection limits of 214 nM for aqueous solutions of $KMnO_4$.[21] That said, since the adopted droplet volumes were excessively large (132 ± 3 nL) and droplet detection rates extremely low (up to 4 Hz), the utility of this system in probing pL-volume droplets at high frequencies is likely to be minimal. Interestingly, the same authors subsequently applied broadband cavity-enhanced absorption spectroscopy to record, in real time, the absorption spectrum of μL-volume aqueous droplets within a microfluidic chip assembly.[22] Although impressive in terms of detection limit, the experimental setup is both complex and costly, and it utilizes extremely large droplet volumes (~6 μL). Accordingly, both of the described techniques are poorly suited for the analysis of segmented flows containing nL−pL volume droplets. More recently, however, a droplet-based microfluidic platform capable of measuring absorbance using a 27 μm path length was described by Deal and Easley.[23] The authors used a combination of confocal microscopy and lock-in detection to probe alternating "sample" and "reference" droplets, achieving a concentration detection limit of 500 nM for Bromophenol blue. Unfortunately, the use of a scanning confocal microscope limits analysis to droplet generation frequencies of 10 Hz, and thus application to high-throughput experimentation is likely to be difficult. Accordingly, it is evident that there exists an unmet need for sensitive and rapid absorption detection in pL-volume droplets within microfluidic flows. To this end, we herein describe the development of a simple, cost-effective optofluidic platform for performing sensitive absorption-based measurements in segmented flows. Specifically, the integration of PDMS waveguides provides for a significant increase in accessible optical pathlengths, thus allowing high-sensitivity absorption measurements.[24] To circumvent droplet-sizing issues associated with fiber-based absorbance measurements,[25] the fabrication of PDMS waveguides results in single-layer microfluidic devices containing channels with dimensions significantly smaller than conventional optical fibers, thus allowing the efficient processing of pL-volume droplets. The ability to create streams of alternating sample and reference droplets allows for continuous referencing of sample signals, and affords concentration detection limits of approximately 400 nM for aqueous solutions of fluorescein. Finally, the described optofluidic system incorporates two synchronized cameras, allowing the simultaneous acquisition of both absorbance and fluorescence data from single, pL-volume droplets in high-throughput.

MATERIALS AND METHODS

Microfluidic Devices. Microfluidic circuits were designed using AutoCAD 2014 (Autodesk, San Rafael, U.S.A.) and printed onto a high-resolution film photomask (Micro Lithography Services Ltd., Chelmsford, U.K.). Master structures were subsequently fabricated on SU-8 (Microchem Corporation, Westborough, U.S.A.) coated silicon wafers via conventional photolithographic methods. Microfluidic devices were manufactured using standard soft-lithographic techniques. Briefly, a 10:1 wt/wt mixture of polydimethylsiloxane (PDMS) base and curing agent (Sylgard 184; Dow Corning, Midland, U.S.A.) was poured over the master structure and cured in the oven at 70 °C for 4 h. The cured PDMS structure was then peeled off the wafer, with inlet and outlet ports being formed using a hole-puncher (Syneo, Florida, U.S.A.). The structured PDMS substrate was then bonded to a 3 mm thick, flat PDMS layer using an oxygen plasma (EMITECH K1000X, Quorum Technologies, East Sussex, United Kingdom). The height of all microchannels was 35 μm, the width of the main channel was 150 μm, and the narrow path width for absorption detection was 26 μm. It should also be noted that two 30 μm wide and 600 μm long dead-end empty channels were placed on each side of the absorption path to minimize and block stray light (Figure S-1). Devices were diced using a homemade guillotine into a rectangular footprint, leaving a gap of less than 800 μm between the side facets and the ends of waveguide channels. Incorporation of such a gap allowed the efficient coupling and detection of light entering and leaving the waveguides. To reduce scattering losses caused by any roughness of the raw facets, the facets were placed vertically onto a layer (200 μm thick) of uncured PDMS spin-coated on a clean silicon wafer. The entire assembly was then baked in the oven at 70 °C for 1 h and disassembled to yield a smooth and transparent surface. This process proved critical in allowing effective coupling of the laser light into and out of the waveguides.

Materials and Reagents. To prevent wetting of microchannel surfaces by the discrete phase, microfluidic devices were flushed with a 2% (by volume) 1*H*,1*H*,2*H*,2*H*-Perfluorooctyl-trichlorosilane (ABCR-chemicals, Karlsruhe, Germany) isopropanol solution for 2 min and air-dried prior to use. A mixture of Fluorinert FC-40 oil (3M, St. Paul, U.S.A.) and fluorinated surfactant (3% w/w and custom synthesized in house) was used as the continuous phase for all experiments. Specified concentrations of fluorescein (Sigma-Aldrich, Buchs,

DOI: 10.1021/acs.analchem.7b03526
Anal. Chem. 2017, 89, 12880−12887

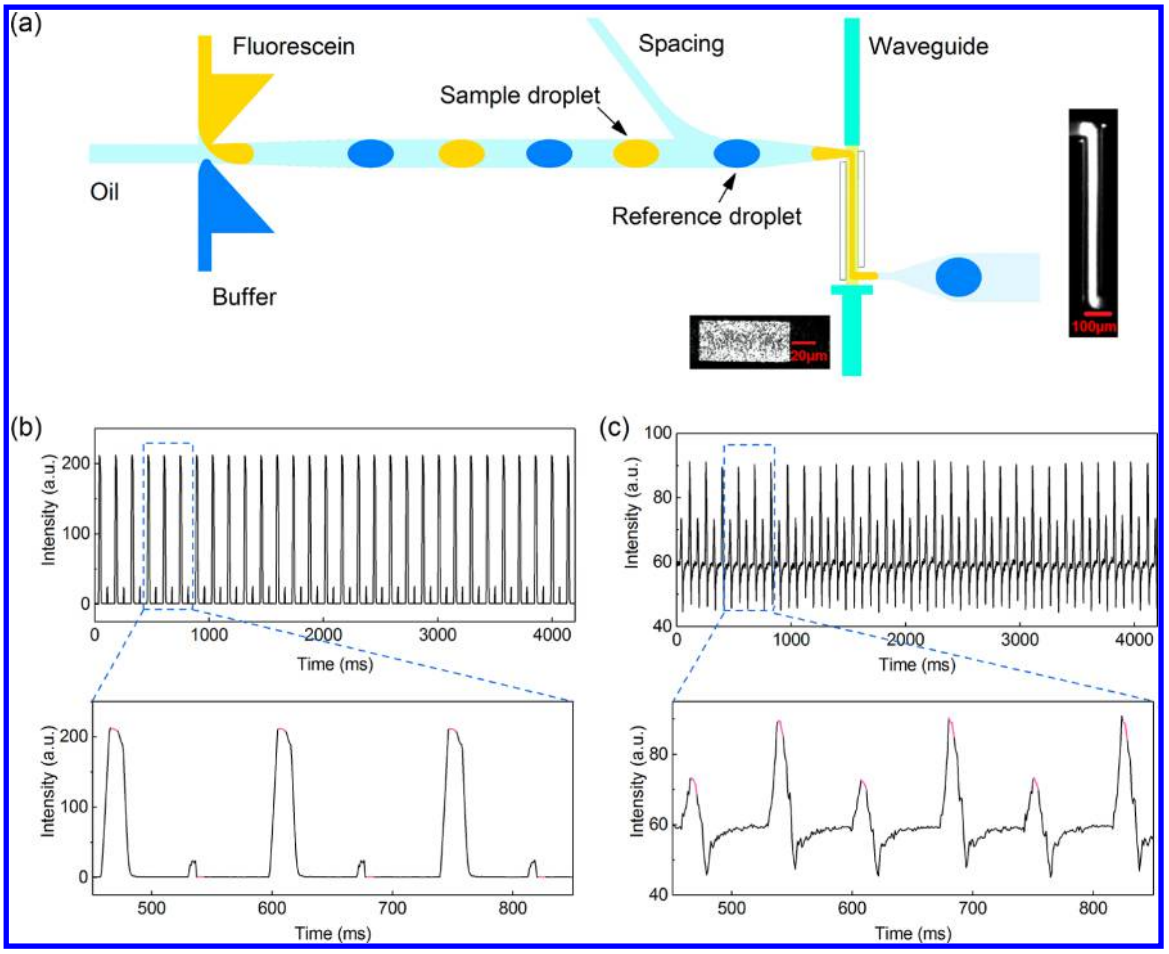

Figure 1. Schematic of the optofluidic platform and proof of principal operation. (a) Schematic of the optofluidic device for droplet analysis. An alternating droplet train of "sample" and "reference" droplets are formed at a double T-junction and motivated toward the droplet detection region, which is flanked by the input and output waveguide channels. (b) Upper panel: fluorescence emission collected over a period of 4 s, reporting 30 "sample" droplets (average intensity = 210.72, 0.1% RSD) and 30 "reference" droplets (0.94, 1.04% RSD). Bottom panel: fluorescence emission collected over a period of 400 ms reporting droplets passing through the optical detection path (highlighted by the blue dash rectangle in the upper panel). High-intensity peaks correspond to the passage of a 460 pL droplet containing 50 μM fluorescein in PBS buffer, and low-intensity peaks correspond to the passage of a 460 pL droplet containing only PBS buffer. (c) Upper panel: Transmitted light time traces of the same droplet train described in (b), collected from the side view of the output waveguide. The average transmitted light intensity for 30 "sample" droplets was 72.46 (0.41% RSD) and 88.79 (0.38% RSD) for 30 "reference" droplets. Bottom panel: transmitted light time traces collected over a period of 400 ms, reporting droplets passing through the optical detection path (highlighted by the blue dash rectangle in the upper panel). The red portions of the plots in both (b) and (c) correspond to times when an individual droplet fully occupies the detection path length.

Switzerland) in deionized water were used to form the dispersed phase. Buffered aqueous solutions of fluorescein (at pHs between 3.83 and 8) were prepared using varying ratios of phosphoric acid and sodium hydroxide (Sigma-Aldrich, Buchs, Switzerland).

Absorbance and Fluorescence Detection. Optical measurements were performed using a custom-built system described in the Supporting Information (Figure S-2). Briefly, a continuous wave laser operating at 488 nm (Sapphire, Coherent, U.K.) was used as the light source for on-chip absorbance measurements. The 700 μm diameter, 10 mW laser beam was reflected by mirrors into a Plan-Neofluar 20× objective 0.4 NA (Carl Zeiss, Jena, Germany) and coupled into one end of the waveguide. The 80 μm wide delivery waveguide was filled with immersion oil (Type A, Nikon, Tokyo, Japan) having a refractive index of 1.515 (i.e., higher than the refractive index of PDMS; n_{PDMS} = 1.412). Nonabsorbed light was collected and transmitted using an identical waveguide. Transmitted light at the end of the delivery waveguide was collected by a Plano N 10× NA 0.25 objective (Olympus, Tokyo, Japan) and imaged through a plano-convex spherical lens (f = 150 mm, Thorlabs, Dachau Germany) onto an 8-bit Genie HM640 CMOS camera (DALSA, Waterloo, Canada) cropped at 640 × 74 pixels and running at 1100 frames/second. A zoom-in lens (Thorlabs, Dachau, Germany) coupled with another 8-bit Genie HM640 CMOS camera (cropped at 1024 × 74 pixels and running at 1100 fps) was placed perpendicular to the chip for both fluorescence detection and brightfield imaging (during droplet production and laser beam alignment). neMESYS low pressure dosing modules (Cetoni GmbH, Korbussen, Germany) were used to motivate all fluids using 1 mL gastight syringes (Hamilton Bonaduz AG, Bonaduz, Switzerland). Tygon tubing (Cole Palmer, Hanwell, U.K.) was used to connect syringes to the inlets of the microfluidic device. For calibration experiments, the droplet alternation frequency was set at 12 Hz (i.e., a droplet generation frequency of 24 Hz) and data were collected over a period of 3 s for each sample concentration. Absorbance measurements were averaged over

DOI: 10.1021/acs.analchem.7b03526
Anal. Chem. 2017, 89, 12880−12887

30 droplets, which corresponds to a total sample volume of 13.8 nL; based on a droplet volume of 460 pL. Control absorbance measurements (of 10 μM fluorescein solutions having pH values between 4 and 8) were performed using the absorbance module of a FluoroMax fluorimeter (HORIBA Scientific, Northampton, U.K.) incorporating either a 1 cm optical path length disposable cuvette or an 800 μm thick custom-made flow-cell.

For pH-sensing experiments, a winding channel section was included subsequent to droplet formation to allow for rapid and efficient mixing of droplet contents via chaotic advection. For on-chip experiments, "reference" droplets were loaded with a 10 μM fluorescein solution at pH 8, while "sample" droplets contained 10 μM fluorescein solutions having pH values between 5 and 8. Subsequent to experiments at a defined pH, the sample syringe was reloaded with the next sample solution, while maintaining alignment of the incident beam with the microfluidic path. Microchannels were washed with buffer for 10 min between each measurement to avoid cross contamination. For pH titration experiments performed on-chip, the two "sample" inlets contained 10 μM fluorescein solution at pH 8 and 0.025 M phosphoric acid, respectively. Component streams were mixed at different ratios to achieve the pH gradients between pH 3.9 and 8. The two reference inlets contained 10 μM fluorescein and buffer solution (both at pH 8), respectively, and were maintained at the same overall volumetric flow rate as the sample inlets. Moreover, buffer was used to compensate for dilution caused by the acid solution on the sample side and ensured identical flow rates and fluorescein concentrations for both reference and sample streams. Inlet channels were washed with buffer for 2 min prior to each new experiment. Finally, droplet frequency, size, and data collection were the same as those in the calibration experiment.

To create user-defined concentration profiles for a series of droplets, the microfluidic device used for pH-sensing experiments was used in conjunction with low pressure neMESYS syringe pumps (CETONI GmbH, Korbussen, Germany). The two reference inlets delivered buffer (without fluorescein) at flow rates of 1 μL/min. One of the sample inlets contained fluorescein at pH 8 and the other a pH 8 buffer solution. The relative flow rates of the two sample streams were adjusted via two complementary periodic flow profiles, while ensuring that the total flow rate was maintained at 2 μL/min. Component flow profiles were consecutively executed over a 2 s period. Two high-speed cameras (8-bit Genie HM640 CMOS camera, DALSA, Waterloo, Canada) were synchronized to obtain image pairs, with an equivalent image rate up to 1000 Hz.

Data Acquisition and Analysis. A custom LabVIEW (National Instruments, Austin, TX) program was used to acquire data as well as synchronize both CMOS cameras. For dual camera synchronization, the frame rate was set to 1000 Hz for 640 × 90 pixels (with a pixel size of 6.5 μm), enabling the simultaneous acquisition of fluorescence and transmission images with a high temporal resolution. An Arduino Uno microcontroller board was used to trigger both cameras at 1000 Hz and data were recorded and processed with custom written LabVIEW software. Data were analyzed using ImageJ (1.47v, National Institutes of Health, Bethesda, U.S.A.). For fluorescence measurements, the region of interest (ROI) was located between the two waveguides as shown in Figure S-3a. Rectangular ROIs having a dimension of 140 × 50 pixels (98 × 35 μm) were selected at the end of the waveguide for analysis of the transmitted light captured by the side camera (Figure S-3b). The mean intensity of each ROI was measured and plotted in sequence, allowing individual droplets to be tracked.

RESULTS AND DISCUSSION

Working Principle and Methodology. The detection part of the optofluidic device is depicted in Figure 1a. The sample and reference streams are delivered in an alternate fashion into the main channel, where they form a pair of droplets entrained in the continuous oil phase. Sample and reference droplets having the same size (460 pL) were formed in an alternate fashion when the sample and reference flow rates are equal. By adopting this approach, the continuous phase does not function as a reference in the absorption measurement, ensuring that the optical effects (caused by refractive index differences between the two phases) are of no consequence. Once steady-state conditions were reached, both the droplet formation frequency and droplet volume were stable for extended times (>1 h without any manual intervention). The optical detection system incorporates a Z-shaped detection path and two liquid-core (PDMS) waveguides. Since the delivery waveguide directs almost the entirety of the incident radiation through the sample (by total internal reflection) the sample liquid should have a higher refractive index than the walls of the surrounding material. While glass (fused silica) capillaries can be used with some solvents, such as dimethyl sulfoxide and toluene, fewer materials, such as low-density Teflon AF 2400,[26] are suitable for use with aqueous samples. In the current experiments, we addressed this issue by forming a PDMS waveguide filled with an immersion oil of higher refractive index than PDMS.[24] We measured both fluorescence (Figure 1b, Figure S-4a) and the light transmitted by the exit waveguide (Figure 1c), using the top and side camera, respectively, for each droplet filled with a fluorescein solution that passes through the detection path. As shown in Figure 1b and Figure S-4c, the peaks reporting reference droplets are characterized by low intensities, identical to the signal contributed by the background (0.91 au and 8.3% RSD) and originate from light scattering at the interface between the spacing oil and droplet. Such scattered contributions disappear when the reference droplet completely fills the channel, thus eliminating any interfaces. The leading edge and plateau portions of sample peaks describe the progressive movement of sample droplets into the optical detection path, while the trailing edge portion describes motion of droplets out of the detection path (Figure S-3a). Light collected by the side view waveguide was detected using a high-speed camera (Figure S-3b) and used to generate the time trace shown in Figure 1c. Since synchronized droplet formation is highly reproducible, the fluorescence signal can be used as a guide in identifying the exact moment when the droplet fully occupies the channel and exhibits a maximal absorbance. Accordingly, counting frames from the top camera allows determination of the exact time period when both reference and sample droplets fully occupy the detection path. According to Beer's Law, the absorbance, A, is given by

$$A = -\log(I_T/I_R) = \varepsilon l c \quad (1)$$

where I_R is the intensity of light that has passed through the reference droplet, I_T is the intensity of light that has passed through the sample droplet, ε is the molar decadic absorption coefficient, l is the optical path length, and c the sample concentration. It should be noted that the spacing oil does exhibit a small signal due to scattering contributions (Figure S-

DOI: 10.1021/acs.analchem.7b03526
Anal. Chem. 2017, 89, 12880−12887

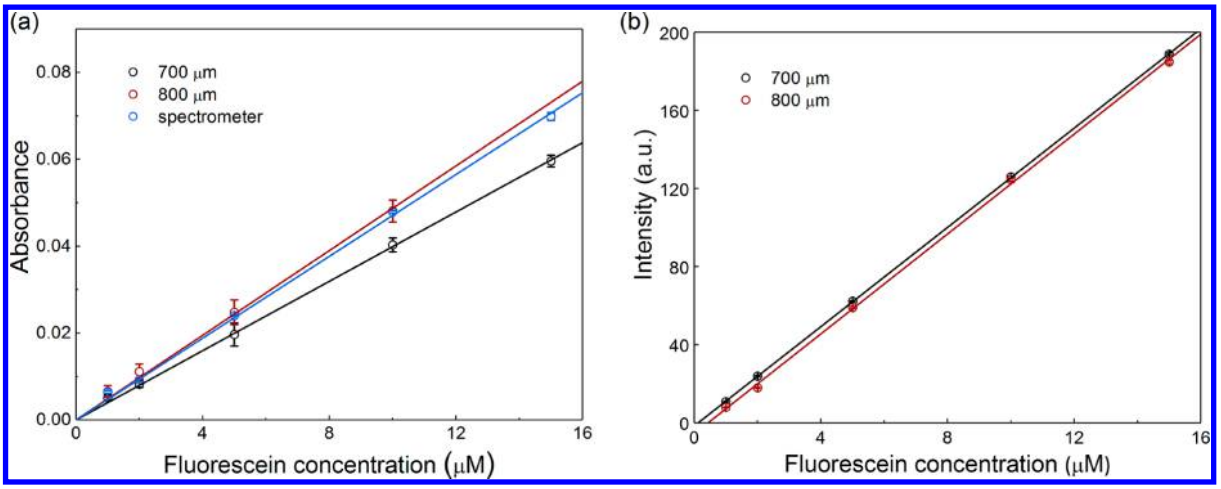

Figure 2. Variation of fluorescence emission and absorbance with concentration. (a) Calibration curves for absorbance detection at a wavelength of 488 nm as a function of fluorescein concentration for different optical pathlengths. Droplet absorbance was measured using the average of 30 different droplet measurements. Absorbance obtained using a benchtop spectrometer with an 800 um path length was measured using the average of five measurements. (b) Calibration curves for fluorescence emission as a function of fluorescein concentration for different optical path lengths.

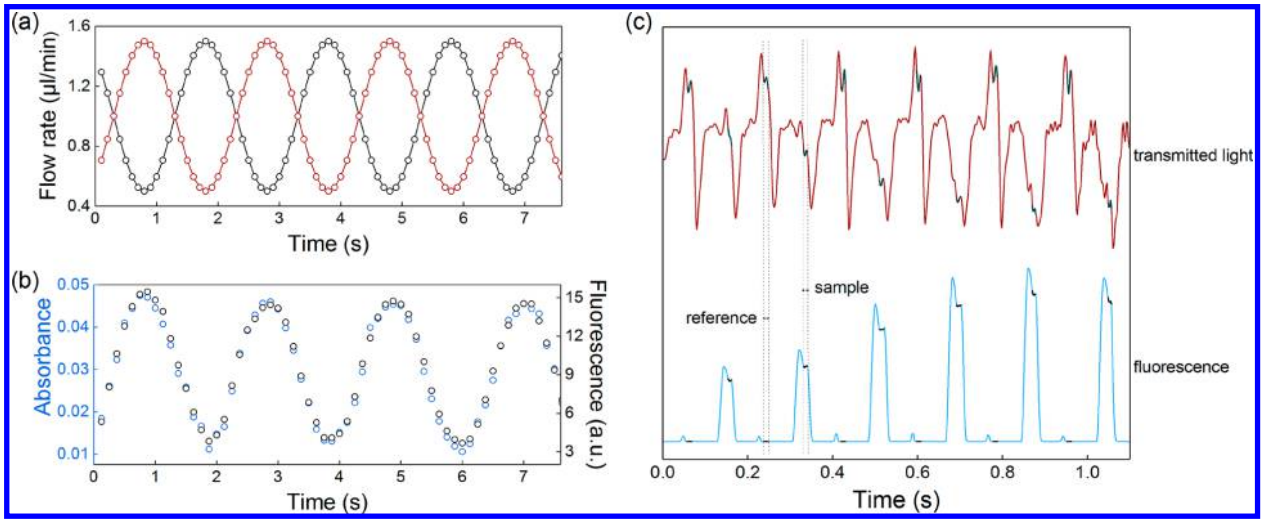

Figure 3. Simultaneous absorbance and fluorescence detection of single droplets flowing through a microfluidic channel. (a) Two sinusoidal complementary flow profiles were applied to the syringe pumps with a period of 2 s (red circles: fluorescein flow, black circles: buffer flow). (b) Correlated absorbance and fluorescence signals enable detection of every single droplet with a unique concentration (chemical payload). (c) Time traces showing a train of droplets moving through the detection path and highlighting the relative changes of transmitted light (red line) and fluorescence (blue line) for the applied flow profiles.

4b) from the nonpurified fluorinated surfactant. Initial experiments utilized a droplet generation frequency of 14 Hz, and thus, the transit time for a single droplet fully occupying the detection path was 27 ms, with a gap between adjacent droplets of 45 ms. By cropping the field of view of the side camera, the frame rate could be increased to 2500 frames/s, and by using an exposure time of 240 μs, we were able to detect light transmission from single droplets at alternation frequencies up to 65 Hz (Figure S-5). As noted, each sample droplet was paired with a reference droplet, thus significantly reducing the impact of frame-to-frame fluctuations of the background and increasing signal-to-noise ratios. The width of the collimated light beam that traverses the detection path is always wider than the width of the microchannel, meaning that both incident and scattered radiation will pass through the substrate to some extent. Such radiation is blocked and collected by the two dead end channels placed 15 mm from the detection path, significantly enhancing detection sensitivity (Figures S-1 and S-4).

Calibration. To fully calibrate our system, pH 7.4 fluorescein solutions at concentrations between 1 and 15 μM were encapsulated into droplets, and their absorbance was measured using an optical path length of either 700 or 800 μm. Figure 2a shows that, as expected, absorbance increases linearly ($R^2 > 0.95$) as a function of concentration for both pathlengths in accordance with Beer's law, with devices containing 700 and 800 μm pathlengths exhibiting concentration detection limits of 406 and 276 nM, respectively. To our knowledge, these values represent the lowest concentration detection limits reported for absorption analysis of single pL-volume droplets (see Table S-1 for an assessment of related prior art). Molar decadic extinction coefficients extracted from the calibration curves were 58 571 ± 481 $M^{-1}\cdot cm^{-1}$ for the 700 μm path length and 61 000 ± 1450 $M^{-1}\cdot cm^{-1}$ for the 800 μm path length. These values are in excellent agreement with a value of 59 125 ± 702 $M^{-1}\cdot cm^{-1}$,

DOI: 10.1021/acs.analchem.7b03526
Anal. Chem. 2017, 89, 12880−12887

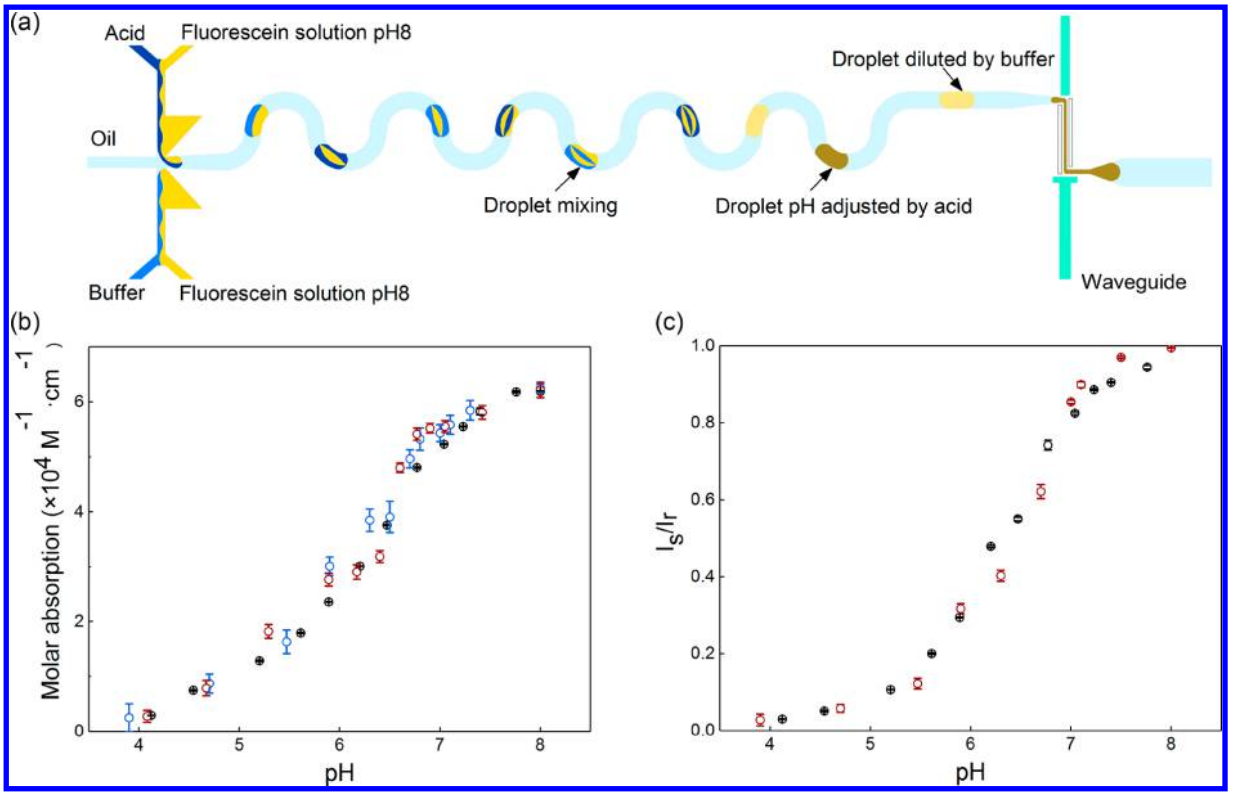

Figure 4. Droplet-based pH-sensing assay platform. (a) Concentrations of fluorescein at different pH values were created by varying the flow rates between acid and fluorescein. A constant amount of buffer and fluorescein solution is added to each reference droplet. Rapid mixing inside the droplets is achieved by chaotic advection and droplets containing different concentrations pass through the optical path length where absorbance and fluorescence are simultaneously detected. (b) Absorbance measurements enable monitoring of pH adjusted on chip (blue circles) and preformed solutions of a certain pH (red circles). Both values strongly correlate to each other and to the measurements obtained for a commercial spectrometer (black circles). (c) Comparison of pH monitoring obtained from fluorescence measurements performed on chip (red circles) and on a commercial spectrometer (black circles).

measured on the conventional spectrometer using an 800 μm path length flow cell.

It should be noted, that although devices integrating an 800 μm path length exhibited lower detection limits than those containing a 700 μm path length, the region of adherence to Beer's Law was superior when using a 700 μm path length. Accordingly, we utilized a 700 μm path length for all subsequent experiments. Finally, Figure 2b reports the variation of fluorescence intensity as a function of concentration between 1 and 15 μM, illustrating a linear relationship between fluorescence intensity and concentration over the entire range (Supplementary Text 1).

Characterization of Concentration Profiles. A key feature of droplet-based microfluidic systems is the ability to vary the chemical payload of large numbers of droplets in a rapid and controllable manner. This suggests significant utility in a range of high-throughput screening applications.[27,28] To this end, we subsequently assessed the ability of our optofluidic platform to generate trains of droplets of varying chemical composition and then to simultaneously extract both fluorescence and absorption signals at high speed. Specifically, subsequent to formation, droplets are motivated within a winding channel section to mix the contained reagents by chaotic advection. Control experiments (data not shown) indicate that reagent mixing is complete before droplets reach the optical detection path. Droplet payloads were controlled by varying the relative flow rates of the component streams containing buffer and fluorescein, through application of two complementary and periodic flow profiles that maintain a constant total flow rate.[29] A variety of flow profiles were tested in regard to extracting the maximum dilution factor, the distribution of droplets with defined concentrations and uniform flow stability; with a sinusoidal function yielding the best results (Figure 3a). This method is easy to implement, flexible, and produces a sequence of droplets, each containing a different chemical composition (Figure 3b). Critically, and as shown in Figure 3b,c, our optofluidic platform is able to detect each droplet and report its unique absorbance and fluorescence signal.

Real-Time pH Titrations. Colorimetric pH indicators are halochromic molecules whose absorbance properties vary as a function of local pH, and they are frequently employed in titrations to determine the extent of a chemical or biological reaction.[30,31] In the current experiments, we compared both absorption and fluorescence measurements obtained either on-chip or from a benchtop spectrometer. On-chip measurements were performed either using buffer whose pH was defined off-chip, or with buffer whose pH was defined on-chip through control of inlet volumetric flow rate ratios. Specifically, because fluorescein has a pK_a of 6.4,[32] its ionization equilibrium leads to a variation in both absorption and emission at pHs between 5 and 9. For pH-sensing experiments, reference droplets were loaded with fluorescein solution at pH 8 and sample droplets loaded with a fluorescein solution of progressively decreasing pH (as shown in Figure 4a). The choice of pH 8 for all reference droplets ensures that the reference droplet will always

DOI: 10.1021/acs.analchem.7b03526
Anal. Chem. 2017, 89, 12880−12887

exhibit higher absorption and fluorescence signals than the "sample" droplet prior to titration. The molar decadic extinction coefficient, ε, of fluorescein can be directly calculated using

$$\log(I_s/I_r) = \log(I_0/I_r) - \log(I_0/I_s) = \varepsilon_r l - \varepsilon_s l \quad (2)$$

where I_s and I_r are the intensities of radiation transmitted by the sample and reference droplet, respectively, and ε_r is the molar decadic extinction coefficient from the reference droplet. This allows extraction of the molar absorption, ε_s. Results obtained using both methods (where pH is adjusted either off-chip or on-chip) are in close agreement, demonstrating the facility to dynamically control and measure pH (Figure 4b). Comparison of pH data obtained via microfluidic experimentation and using a commercial spectrometer similarly exhibit a strong correspondence, further confirming the capability of the optofluidic platform in performing quantitative and precise pH measurements. Moreover, it is also noted that emission ratios (I_s/I_r) captured using the camera placed above the optical detection pathway are in excellent agreement with measurements performed using a benchtop fluorimeter (Figure 4c).

CONCLUSIONS

Herein, we have established a simple and cost-effective method to measure the absorbance of single pL-volume droplets at high speed. The key innovation in the described work is the integration of high-sensitivity, on-chip waveguides with droplet-based manipulations, which enhances optical pathlengths and further allows the simultaneous measurement of both absorbance and fluorescence from flowing droplets. Critically, such an approach exploits the small sample volumes representative of droplet-based microfluidic systems (around 400 pL) and thus reduces sample consumption with respect to conventional absorbance techniques. Results demonstrate a high degree of experimental accuracy for single-droplet absorbance measurements and a concentration limit of detection of 400 nM for aqueous solutions of fluorescein. Analysis of transmitted light intensities using the side view waveguide, indicates a linear dynamic range of 1−15 μM for droplet alternation frequencies of up to 65 Hz. On a more practical level, the described method provides for sensitive, reliable, and precise pH sensing using a simple setup and standard laboratory equipment. Refinement of the optofluidic system through adoption of a more sensitive (16-bit pixel depth) camera and integration of on-chip PDMS microlenses, will engender significant improvements in both dynamic range and concentration detection limits. Finally, it should be noted that the ability to perform sensitive and simultaneous absorbance and fluorescence measurements is of significant utility in experiments that require online read out of analyte concentrations.

ASSOCIATED CONTENT

Supporting Information

The Supporting Information is available free of charge on the ACS Publications website at DOI: 10.1021/acs.analchem.7b03526.

Microfluidic channel designs; details of optical detection system; fluorescence and transmitted light images of a sample and reference droplet and oil with surfactant; droplet absorbance calibration curve at high frequencies; comparison of the different optical absorbance approaches in microfluidic platforms; theoretical assessment of the linear relationship between fluorescent intensity and concentration of fluorophore (PDF)

AUTHOR INFORMATION

Corresponding Authors

*E-mail: andrew.demello@chem.ethz.ch.
*E-mail: stavros.stavrakis@chem.ethz.ch.

ORCID

Andrew deMello: 0000-0003-1943-1356

Notes

The authors declare no competing financial interest.

REFERENCES

(1) Srisa-Art, M.; deMello, A. J.; Edel, J. B. *Anal. Chem.* **2007**, *79*, 6682−6689.
(2) Guo, F.; Lapsley, M. I.; Nawaz, A. A.; Zhao, Y.; Lin, S. C.; Chen, Y.; Yang, S.; Zhao, X. Z.; Huang, T. J. *Anal. Chem.* **2012**, *84*, 10745−10749.
(3) Jeffries, G. D.; Lorenz, R. M.; Chiu, D. T. *Anal. Chem.* **2010**, *82*, 9948−9954.
(4) Rane, T. D.; Puleo, C. M.; Liu, K. J.; Zhang, Y.; Lee, A. P.; Wang, T. H. *Lab Chip* **2010**, *10*, 161−164.
(5) Dittrich, P. S.; Jahnz, M.; Schwille, P. *ChemBioChem* **2005**, *6*, 811−814.
(6) Srisa-Art, M.; deMello, A. J.; Edel, J. B. *J. Phys. Chem. B* **2010**, *114*, 15766−15772.
(7) Gielen, F.; van Vliet, L.; Koprowski, B. T.; Devenish, S. R.; Fischlechner, M.; Edel, J. B.; Niu, X.; deMello, A. J.; Hollfelder, F. *Anal. Chem.* **2013**, *85*, 4761−4769.
(8) Lignos, I.; Protesescu, L.; Stavrakis, S.; Piveteau, L.; Speirs, M. J.; Loi, M. A.; Kovalenko, M. V.; deMello, A. J. *Chem. Mater.* **2014**, *26*, 2975−2982.
(9) Hassan, S.; Nightingale, A. M.; Niu, X. *Analyst* **2016**, *141*, 3266−3273.
(10) Ohlsson, P. D.; Ordeig, O.; Mogensen, K. B.; Kutter, J. P. *Electrophoresis* **2009**, *30*, 4172−4178.
(11) Löbbecke, S.; Ferstl, W.; Panić, S.; Türcke, T. *Chem. Eng. Technol.* **2005**, *28*, 484−493.
(12) Suhyeon, K.; Weonseop, K.; Jong, H. H. *J. Chromatogr. A* **1994**, *680*, 109−116.
(13) Liang, Z.; Chiem, N.; Ocvirk, G.; Tang, T.; Fluri, K.; Harrison, D. J. *Anal. Chem.* **1996**, *68*, 1040−1046.
(14) Mogensen, K. B.; Petersen, N. J.; Hübner, J.; Kutter, J. P. *Electrophoresis* **2001**, *22*, 3930−3938.
(15) Ro, K. W.; Lim, K.; Shim, B. C.; Hahn, J. H. *Anal. Chem.* **2005**, *77*, 5160−5166.
(16) Song, W.; Yang, J. *Lab Chip* **2012**, *12*, 1251−1254.
(17) Llobera, A.; Demming, S.; Wilke, R.; Buttgenbach, S. *Lab Chip* **2007**, *7*, 1560−1566.
(18) Zhang, L.; Wang, P.; Xiao, Y.; Yu, H.; Tong, L. *Lab Chip* **2011**, *11*, 3720−3724.
(19) Rushworth, C. M.; Jones, G.; Fischlechner, M.; Walton, E.; Morgan, H. *Lab Chip* **2015**, *15*, 711−717.
(20) Autour, A.; Ryckelynck, M. *Micromachines* **2017**, *8*, 128.
(21) James, D.; Oag, B.; Rushworth, C. M.; Lee, J. W. L.; Davies, J.; Cabral, J. T.; Vallance, C. *RSC Adv.* **2012**, *2*, 5376−5384.
(22) Neil, S. R.; Rushworth, C. M.; Vallance, C.; Mackenzie, S. R. *Lab Chip* **2011**, *11*, 3953−3955.
(23) Deal, K. S.; Easley, C. J. *Anal. Chem.* **2012**, *84*, 1510−1516.
(24) Fei, P.; Chen, Z.; Men, Y.; Li, A.; Shen, Y.; Huang, Y. *Lab Chip* **2012**, *12*, 3700−3706.
(25) Jakiela, S.; Kaminski, T. S.; Cybulski, O.; Weibel, D. B.; Garstecki, P. *Angew. Chem., Int. Ed.* **2013**, *52*, 8908−8911.
(26) Cho, S. H.; Godin, J.; Lo, Y. H. *IEEE Photonics Technol. Lett.* **2009**, *21*, 1057−1059.
(27) Niu, X.; deMello, A. J. *Biochem. Soc. Trans.* **2012**, *40*, 615−623.

DOI: 10.1021/acs.analchem.7b03526
Anal. Chem. 2017, 89, 12880−12887

(28) Dressler, O. J.; Casadevall i Solvas, X.; deMello, A. J. *Annu. Rev. Anal. Chem.* **2017**, *10*, 1−24.
(29) Hess, D.; Rane, A.; deMello, A. J.; Stavrakis, S. *Anal. Chem.* **2015**, *87*, 4965−4972.
(30) Yao, W.; Byrne, R. H. *Environ. Sci. Technol.* **2001**, *35*, 1197−1201.
(31) Nakayama-Ratchford, N.; Bangsaruntip, S.; Sun, X.; Welsher, K.; Dai, H. *J. Am. Chem. Soc.* **2007**, *129*, 2448−2449.
(32) Sjöback, R.; Nygren, J.; Kubista, M. *Spectrochim. Acta, Part A* **1995**, *51*, L7−L21.

DOI: 10.1021/acs.analchem.7b03526
Anal. Chem. 2017, 89, 12880−12887